Cav03-OS-1-004

Fifth International Symposium on Cavitation (Cav2003)
Osaka, Japan, November 1-4, 2003

A Virtual Single-Phase Natural Cavitation Model And its Application to Cav2003 Hydrofoil

Qiao Qin
St. Anthony Falls Laboratory,
University of Minnesota
qinx0007@umn.edu

Charles C.S. Song
St. Anthony Falls Laboratory,
University of Minnesota
csssong@aol.com

Roger E.A. Arndt
St. Anthony Falls Laboratory,
University of Minnesota
arndt001@umn.edu

Abstract

Cavitating flows are notoriously complex because they are highly turbulent and unsteady flows involving two species (liquid/vapor) with a large density difference. These features pose a unique challenge to numerical modeling works. A simplified virtual single-phase natural cavitating model recently developed and applied to NACA series hydrofoils, such as 0015 and 4412, has been shown capable of capturing the primary dynamics of complex cavitating flows. Details of this model, including assumptions, governing equations, turbulence modeling, numerical method, and boundary conditions will first be presented. Its application to the Cav2003 hydrofoil will then be carried out. Most of the results asked for in this specific organized session will be presented.

A Brief Literature Review

In liquid flows, cavitation generally occurs if the pressure drops below the vapor pressure and consequently the negative pressures are relieved by means of forming gas filled or gas and vapor filled cavities (Batchelor, 1967). Therefore, cavitation is the phenomenon of the formation, growth and rapid collapse of bubbles. It may occur through the formation of bubbles or cavities in the liquid, or it can be a result of the enlargement of cavities that are already present in the bulk liquid (Shah *et al*, 1999). Cavitation research has long been important in ship propellers, pump impellers, turbines and hydrofoils where cavitation is often unavoidable.

Cavitation has various stages and types, such as traveling cavitation, sheet cavitation, sheet/cloud cavitation, vortex cavitation and supercavitation. Traveling cavitation is composed of individual transient cavities or bubbles that form in the liquid and move with the liquid as they expand, shrink, and then collapse. It typically occurs on hydrofoils at the early stage of cavitation with small angle of attack. Sheet cavitation is characterized by a continuous liquid/vapor interface that is attached to a surface of certain object. This liquid/vapor interface can be either glossy or rough. The onset of sheet cavitation is approximately fixed. Sheet cavitation can be further subcategorized as steady and unsteady although cavitation phenomenon itself is intrinsically unsteady. The steady sheet cavitation is defined such that the cavity length is fairly constant in time except that the cavity fluctuation is only limited within the closure region. Correspondingly, the unsteady sheet cavitation (also called sheet/cloud cavitation) means that the length of sheet cavitation varies drastically with time. This unsteady sheet cavitation is periodically broken down and shed into the wake with the form of a vapor cloud containing numerous micro bubbles. Callenaere *et al* (2001) found experimentally that this instability is due to the development of a re-entrant jet at the back of the cavity. Vortex cavitation is often observed in the cloud, which is caused by vorticity shed into the flow field. Supercavitation forms when the cavity length exceeds the length of the body. Supercavitation can be either natural cavitation or ventilated cavitation.

Cavitation by definition involves two species, liquid and vapor/gas. A number of discontinuities, such as heat conduction, viscosity, compressibility, surface tension, mass transfer, diffusivity and temperature occur at the liquid/vapor interface, and these discontinuities have not been well quantified. Cavitation is also found interactive with fluid turbulence (Gopalan and Katz, 2000; Song and He, 1998). These are the mathematical challenges in cavitation modeling. Because of its complex nature, there is no single mathematical cavitation model in literature that can take care of all the above factors. Certain degree of assumptions and/or simplifications has to be made to accommodate different application needs.

The bulk of cavitation modeling deals with steady sheet cavitation, its size and shape. It assumes the cavitation region as a large bubble with a distinct liquid/vapor interface. Basically three assumptions are made for a cavitation bubble: the bubble boundary is a free surface; the pressure inside the bubble is constant and equals to the vapor pressure of its corresponding liquid; the closure region of the bubble can be approximated by a wake model. Works in this area include potential flow based models (Brennen, 1969; Furness and Hutton, 1975; Pellone and Rowe, 1981; Lemonnier and Rowe, 1988; Uhlman, 1987; Ingber and Hailey, 1991; Lee *et al*, 1992; and Kinnas and Fine, 1993) and Euler and Navier-Stokes equation based models (Chen and Heister, 1994; Deshpande *et al*, 1997). Although being drastically simplified, these models are able to predict the wall detachment point, bubble forebody and solid wall pressure distribution fairly well. The deficiencies of these models, however, are obvious: they are only limited to the stable sheet cavitation case in a quasi-steady state; no turbulence model is included; no cavitation model is involved in a strict sense; wake model is not physical;

it is limited to 2D computation because of the difficulty to track 3D liquid/vapor interface.

Instead of attempting to distinguish species between liquid and vapor and to track their interface, an alternative strategy is to treat cavitating flows as a homogeneous two-phase mixture of liquid and vapor. This treatment neglects the possible slip between liquid and vapor interface and regards liquid/vapor and their mixture as a single fluid that satisfies Navier-Stokes equation. The advantages are: models with this strategy can, in principle, cover all types of cavitation, including traveling cavitation, sheet and sheet/cloud cavitation, and supercavitation; turbulence model can be easily included.

The key challenge here is how to define the mixed density of the single fluid. One approach is to introduce the concept of volume fraction or volume of fluid (VOF, a notation employed by some commercial software such as FLUENT). The mixed density and viscosity of the single fluid is defined as

$$\rho = \alpha\rho_v + (1-\alpha)\rho_l \,, \tag{1}$$

and

$$\mu = \alpha\mu_v + (1-\alpha)\mu_l \,. \tag{2}$$

Where α is the volume fraction of vapor and subscripts *v* and *l* denote vapor and liquid, respectively. The following additional transport equation is often solved to determine the volume fraction α

$$\frac{\partial(\alpha\rho)}{\partial t} + \frac{\partial(\alpha\rho u_i)}{\partial x_i} = So \,, \tag{3}$$

where *So* is the source term that is used to model phase transition. Kubota e*t al* (1992) relates the volume fraction α to the motion of bubbles in the flow

$$\alpha = n\frac{4}{3}\pi R_b^3 \,, \tag{4}$$

where, *n* is the constant number of bubbles pre-specified in the flow, R_b is the bubble radius that is governed by Rayleigh-Plesset equation based on the pressure field. Chen and Heister (1996) extended this idea to the variable number of bubbles which was not required to be specified *a priori*. Merkle *et al* (1998) introduced the mass transfer between vapor and liquid as the source term in equation (3) that was used in chemically reacting flows. Kunz *et al* (1999) followed the same idea as Merkle *et al* (1998) and detailed the evaporation process $\dot{m}^-$ and condensation process $\dot{m}^+$ as follows

$$\dot{m}^- = \frac{C_{dest}\rho_v\alpha\min[0, p-p_v]}{\left(\frac{1}{2}\rho_l U_\infty^2\right)t_\infty} \,, \tag{5}$$

and

$$\dot{m}^+ = \frac{C_{prod}\rho_v\alpha^2(1-\alpha)}{t_\infty} \,. \tag{6}$$

Where, C_{dest} and C_{prod} are empirical constants for evaporation and condensation transfer process, respectively.

A simpler approach is based on the equation of state that relates pressure and density. A general equation of state can be written as

$$\rho = f(P,T) \,. \tag{7}$$

By assuming the cavitating process to be isothermal (barotropic), mixed density is simply a function of local pressure. Delannoy and Kueny (1990) pioneered this work. They found that the compressibility of the vapor and liquid was not important except during the final phase of collapse and hence adopted three states of the mixed density: two incompressible parts in both ends (pure liquid and pure vapor) and the transition part following a sine law, $\rho = f(P)$. Chen and Heister (1996) derived a time and pressure dependent density

$$\frac{D\rho}{Dt} = C(P - P_v) \,, \tag{8}$$

where *C* is a constant. Hoeijmakers *et al* (1998) inherited the similar idea as Delannoy and Kueny (1990). Song and He (1998) used the following fifth order polynomial to simulate the cavitating process

$$\rho = \sum_{i=0}^{5} A_i P^i \,. \tag{9}$$

Here, coefficients A_i were so chosen that the density decreased sharply as soon as the pressure dropped below the critical (vapor) pressure.

Cavitating flows are also highly dynamic and turbulent. Only part of Navier-Stokes equation based single-fluid cavitation models includes a turbulence model. Popularly used turbulence models are either various version of *k-ε* model for Reynolds Averaged Navier-Stokes (RANS) equation (Kunz *et al*, 2000; Senocak and Shyy, 2002) or turbulent viscosity model for Large Eddy Simulation (LES) (Song and He, 1998). Coutier-Delgosha *et al* (2003) offered an influence evaluation of various *k-ε* turbulence models on the numerical simulation of unsteady cavitation and concluded that the fluid compressibility has a strong effect on the turbulence structure and must be taken in to account when unsteady cavitating flows were simulated. A general understanding of the interaction between turbulence and cavitation is still well beyond our grasp.

It is worth mentioning that, as the large density difference exists between liquid and gas, the pseudo-density of the single fluid varies dramatically between liquid density and vapor density, which frequently leads to the numerical instability.

Governing Equations

It is well known that unsteady compressible flows with small Mach numbers are very difficult to compute due to a great disparity between the speed of sound and the speed of flow convection. More importantly, small amount of compressibility plays dominant role in highly unsteady flows (Song, 1996). If the fluid is assumed to be incompressible, the resulting equation can no longer be used to represent highly time-dependent flows. Song and Yuan (1988) proposed a weakly compressible flow model, which works equally well for both steady and unsteady flow problems. The general equation for sound speed, *a,* is

$$\frac{\partial p}{\partial \rho} = a^2 \,. \tag{10}$$

Substitution of (10) into the equation of continuity yields a conservative form of equation for p,

$$\frac{\partial p}{\partial t} + \nabla \bullet \rho a^2 \vec{V} = \rho \vec{V} \bullet \nabla a^2 \,. \tag{11}$$

The density of fluid ρ and the speed of sound a are, in general, functions of time t and space. However, when the Mach number is small, the variation of ρ and a is very small. Therefore, the speed of sound can be assumed constant and the density of fluids becomes a linear function of pressure. In this case, the above equation (11) can be simplified as

$$\frac{\partial p}{\partial t} + \nabla \bullet \rho_0 a_0^2 \vec{V} = 0 \ , \qquad (12)$$

where the subscript "$_0$" represents a reference quantity. Note that the first term is proportional to $M^2 S_t$, which is negligible when M is small and S_t is not too large. In this case equation (12) reduces to the continuity equation for incompressible flow. But if the flow is highly unsteady or S_t is large, the time derivative term is not negligible and both terms should be kept. Flows governed by equation (12) are called weakly compressible flows.

When cavitation occurs, the density drops sharply as soon as the pressure is below the vapor pressure. To simulate this vaporization phenomenon, Song and He (1998) formulated a so-called virtual single-phase flow model as follows

$$\rho = \sum_{i=0}^{5} A_i p^i \qquad \text{for} \qquad p_\varepsilon < p < p_c \ . \qquad (13)$$

The coefficients A_i are so chosen that the resulting pressure-density curve has a desirable shape. Equation (13) smoothly joins with the weakly compressible flow pressure-density relationship at the critical pressure p_c

$$p - p_0 = a_0(\rho - \rho_0) \qquad \text{for} \qquad p_c \le p \ . \qquad (14)$$

Since the Mach number of the flow inside a cavity may not be small, the fully compressible flow model with barotropic assumption is used. In addition, the heat transfer may not be negligible across the liquid/vapor interface due to the latent heat of vaporization. However, as we focus on the cavitation characteristics in the macro sense in the present study, thermodynamic effects remain excluded.

The general conservation form of equations of continuity and motion can therefore be summarized as follows

$$\frac{\partial U}{\partial t} + \nabla \bullet \vec{Q} = S \ , \qquad (15)$$

where,

$$U = \begin{bmatrix} p \\ \rho u \\ \rho v \\ \rho w \end{bmatrix}, \quad Q_1 = \begin{bmatrix} \rho a^2 u \\ \rho u^2 + p - \tau_{xx} \\ \rho uv - \tau_{xy} \\ \rho uw - \tau_{xz} \end{bmatrix},$$

$$Q_2 = \begin{bmatrix} \rho a^2 v \\ \rho vu - \tau_{yx} \\ \rho v^2 + p - \tau_{yy} \\ \rho vw - \tau_{yz} \end{bmatrix}, Q_3 = \begin{bmatrix} \rho a^2 w \\ \rho wu - \tau_{zx} \\ \rho wv - \tau_{zy} \\ \rho w^2 + p - \tau_{zz} \end{bmatrix},$$

$$S = \begin{bmatrix} \rho u \dfrac{\partial a^2}{\partial x} + \rho v \dfrac{\partial a^2}{\partial y} + \rho w \dfrac{\partial a^2}{\partial z} \\ 0 \\ 0 \\ 0 \end{bmatrix}. \qquad (16)$$

Large-Eddy Simulation Approach and Turbulence Model

Turbulent flows are composed of eddies. The scales of eddies ranges from those comparable to the domain of interest down to the Kolmogorov dissipation scale. To resolve all the scales in the flow of engineering interest remains impractical with current digital resources. There is evidence that large scales of motion have vigorous interaction with the mean flow and they strongly depend on the flow geometry and the nature of the flow, while the small scales (or Sub-grid Scale, SGS) of the motion as the production of a nonlinear interaction of large eddies tend to be more universal and homogeneous and have less influence on mean flows. The essence of Large-Eddy Simulation (LES) is to explicitly resolve the large scales of the motion and, in the meanwhile, model the small scales (SGS) of the motion in the flow. The LES approach has become increasingly popular in the community of CFD because of this nature.

After applying a Favre-filtering operation to equation (15), and neglecting the non-linearity of the viscous stresses (Piomelli 1999), an extra non-linear term occurs,

$$\tau_{Sij} = \overline{\rho}(\overline{u_i u_j} - \overline{u_i}\,\overline{u_j}) \, , \qquad (17)$$

which are called Sub-grid Scale (SGS) stresses and must be modeled. Here quantities with overbars stand for filtered quantities, or large scale quantities. The overbars will be dropped hereafter for convenience.

A popularly used SGS model is the eddy-viscosity model of the form

$$\tau_{Sij} = -2\rho \upsilon_t S_{ij} \, , \qquad (18)$$

that relates the SGS stresses τ_{Sij} to the Favre-filtered strain-rate tensor S_{ij}.

In most cases the equilibrium assumption is made to further simplify the problem and an algebraic model for the eddy viscosity is obtained

$$\upsilon_t = (C_s \Delta)^2 \, | S | \, S_{ij} \, , \qquad (19)$$

where Δ is the grid size and C_s is the Smagorinsky constant and takes values between 0.1 and 0.23, depending on the flow. This model is also known as the Smagorinsky model. However, the Smagorinsky constant C_s must be decreased in the presence of shear, near solid boundaries or in transitional flows. This can be done by incorporating another damping function. Moin and Kim (1982) proposed the following modification

$$\upsilon_t = (C_s D_f \Delta)^2 \, | S | \, S_{ij} \, , \qquad (20)$$

where D_f is a nondimensional damping factor. This damping factor will only affect the turbulent viscosity near the solid wall.

Despite the lack of universality of the Smagorinsky constant and some other defects, the eddy viscosity model is still a very useful model for LES. To dynamically obtain the Smagorinsky coefficient, Germano (1991) proposed a dynamic eddy viscosity model. In the dynamic model, the Smagorinsky coefficient is determined as the calculation progresses, based on the energy content of the smallest resolved scale. This is accomplished by introducing a secondary test filter whose width is larger than the grid filter width. Two drawbacks, however, exist behind the dynamic model. One is that the filtering process of the second test filter is considerably more expensive. The other is that the dynamic model is proved not dissipative enough near the wall while Smagorinsky model is too dissipative. The dynamic model, therefore, goes to the other extreme, compared to the Smagorinsky model, in this sense. A more sophisticated SGS model needs to be investigated later on.

Numerical Method

The finite volume method with a 2nd order accurate MacCormack's predictor-corrector numerical scheme is used. By integrating equation (18) over each finite volume, and using the divergence theorem, one can get

$$\frac{\partial U}{\partial t} + \frac{1}{\forall}\iint_A \vec{n} \bullet \vec{Q} dA = \overline{S} . \qquad (21)$$

Here U is volume averaged quantity placed at the center of the volume. To meet the numerical stability requirement, the time increment is limited by the following:

$$\Delta t \le C_r \frac{\forall}{|\vec{u} \bullet \vec{A}| + a|A|}, \qquad (22)$$

where C_r is the Courant stability factor, which is less than one but greater than zero.

Mesh Structure and Boundary Conditions

A three dimensional Large Eddy Simulation (LES) code with eddy viscosity turbulence model is used to simulate the two dimensional Cav2003 hydrofoil, at 7 degree angle of attack. Only three computational grids plus two phantom grids are used in the span wise direction for a two dimensional effort. The flow configuration is sketched in Fig. 1, which is exactly the same geometry as specified in Franc and Schnerr (2002). Since the flow close to the hydrofoil surface is of particular importance in the current study, the mesh structure in the computational domain deliberately reflects this concern by heavily clustering the mesh close to the solid surface of the hydrofoil so that the fine mesh encloses the foil (Fig. 2).

The commonly used far-field boundary conditions (zero gradients) are implemented at upstream and downstream boundaries. In addition, the inflow stream wise velocity is assigned and the downstream cross-sectional-averaged pressure rather than the pressure at a fixed point, which was specified by Franc and Schnerr (2002), is controlled as the reference pressure. Note that controlling the pressure at a fixed point is not physically possible nor numerically stable. Only by controlling the average pressure can leave sufficient flexibility to enable the pressure at any fixed point to vary with time reflecting turbulence. These conditions are summarized as follows

Upstream

$$\frac{\partial u_i}{\partial x} = \frac{\partial P}{\partial x} = 0 \ \ (i=1,2,3), \quad \text{and} \quad u_1 = U_0, \qquad (23)$$

Downstream

$$\frac{\partial u_i}{\partial x} = \frac{\partial P}{\partial x} = 0 \quad (i=1,2,3) \quad \text{and} \quad \overline{P} = P_{reference} . \qquad (24)$$

A full-slip boundary condition is used at both the upper and lower walls as well as at the artificial boundaries at the ends of the span to avoid the occurrence of viscous boundary layers. Although the mesh is heavily clustered near the solid surface, it is still not fine enough to resolve the thin boundary layer in the non-cavitating scenario. A partial-slip boundary condition (Song 1999) is therefore applied. When cavitation occurs, however, the boundary layer becomes thicker and hence the partial-slip automatically becomes no-slip. In either case, the pressure condition on foil solid wall is specified in the following way

$$\frac{\partial P}{\partial n} = 0 . \qquad (25)$$

As in the specification (Franc and Schnerr, 2002), the upstream free stream velocity U_0 is taken as 6m/s. The chord length c is taken as 0.1m. The Reynolds Number based upon chord length is therefore 6×10^5. The turbulence level 0.1% is also superimposed into a uniform velocity at the upstream inlet.

Computational Results

Lift Coefficient. The lift coefficient of a 2D hydrofoil is defined as

$$C_l = \frac{L}{\frac{1}{2}\rho U_0^2 c}, \qquad (26)$$

where L equals the net lift force per unit span working on the hydrofoil, U_0 is the free stream velocity and c is the hydrofoil chord length.

The time series of lift coefficient under non-cavitating condition is presented in figure 3. Clearly shown in this figure is that the lift coefficient under non-cavitating condition fluctuates about its mean value because the flow on the suction side starts to separate from the hydrofoil surface at about 70% of the chord length. The boundary layer separation is an unsteady phenomenon leading to lift fluctuation. Figure 4 is an instantaneous velocity distribution that illustrates this flow separation phenomenon, which is close to the trailing edge of the suction side. Careful observation of velocity vector field indicates that the separated flow consists of formation and shedding of coherent eddies.

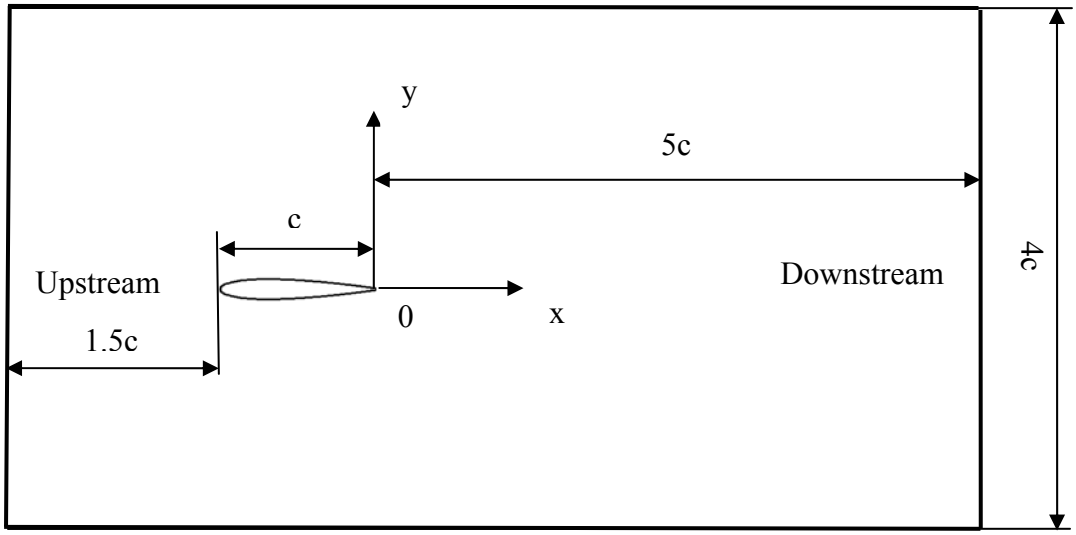

Fig. 1 Computational flow configuration

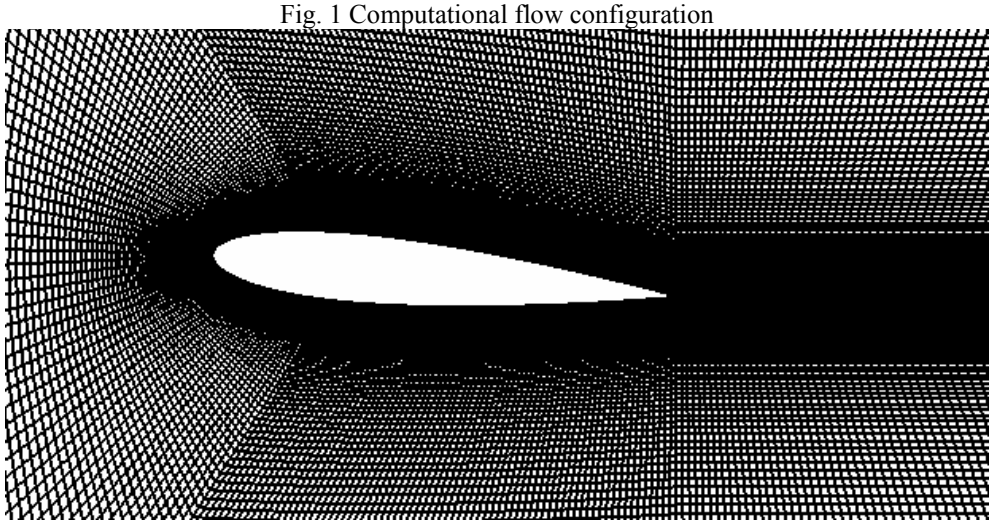

(a) The grid system enclosing the hydrofoil

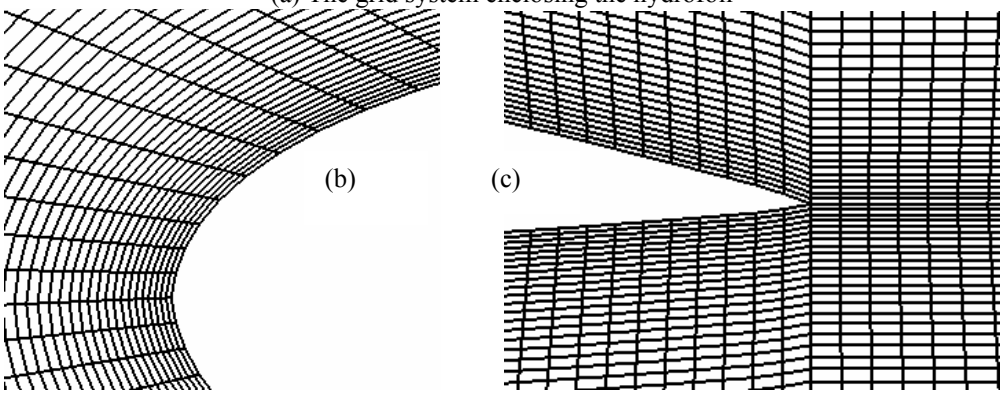

Fig. 2 Grid system surrounding the NACA 0015 hydrofoil at 6 degree angle of attack
(b) A close-up near the leading edge, (c) A close-up near the trailing edge

The time averaged lift coefficients under both non-cavitating and cavitating conditions are listed as follows (table 1).

Table 1 Time averaged lift coefficients under non-cavitating and cavitating conditions

	No cavitation	σ = 0.8	σ = 0.4
Time-averaged lift coefficient	0.646	0.359	0.183

Pressure Distribution. Pressure coefficient is defined as

$$C_p = \frac{P - P_0}{\frac{1}{2}\rho U_0^2}, \tag{27}$$

where P_0 is the upstream reference pressure.

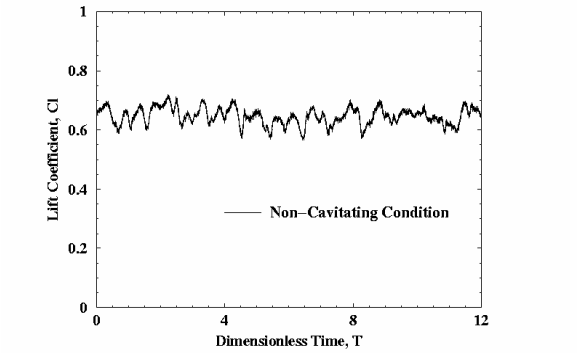

Fig. 3 Time series of lift coefficient under non-cavitating condition

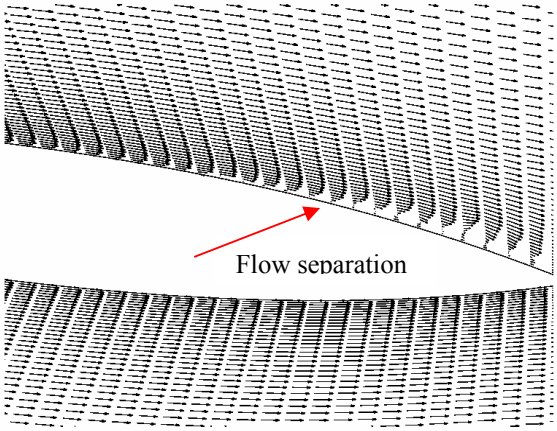

Fig. 4 Instantaneous velocity distribution near the trailing edge showing flow separation under non-cavitating condition at 7 degree angle of attack

The time averaged pressure coefficient under non-cavitating condition is plotted at figure 5. A couple of findings for this hydrofoil are summarized as follows. The cavitation inception number by definition is the negative of the minimum pressure coefficient, if the tensile strength is neglected. It is found in this case the cavitation inception number is 3.75. As the leading edge radius is smaller, the pressure coefficient on the suction side has much sharper peak than that of hydrofoils with relatively larger leading edge radius (NACA 0015, for instance, see Qin *et al*, 2003a). This leads to larger adverse pressure gradient and boundary layer separation. This may also be the reason why the average lift coefficient is some what smaller than the theoretical value of $2\pi\alpha$ for a flat plate.

The time averaged pressure coefficient under cavitating conditions (σ=0.8, 0.4) are presented in figures 6 and 7, respectively. It is noted that the pressure within the cavity is approximately constant, which is consistent with the experimental data. In addition, there is a zone of negative pressure on the pressure side near the trailing edge. Thus, there is a zone near the trailing edge where pressure on the suction side is greater than that of the pressure side contributing to negative lift. Under the partial cavity condition, the smaller the cavitation number the greater the lift reduction of the type just described exists.

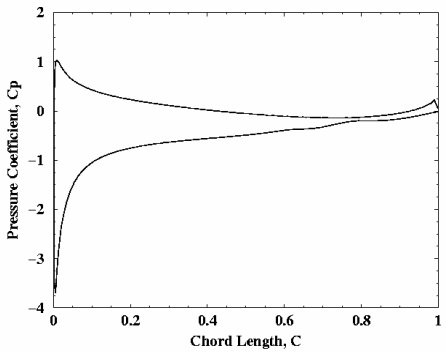

Fig. 5 Time averaged pressure coefficient under non-cavitating condition

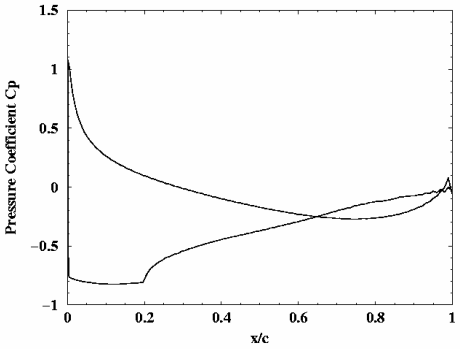

Fig. 6 Time averaged pressure coefficient under cavitating condition (σ =0.8)

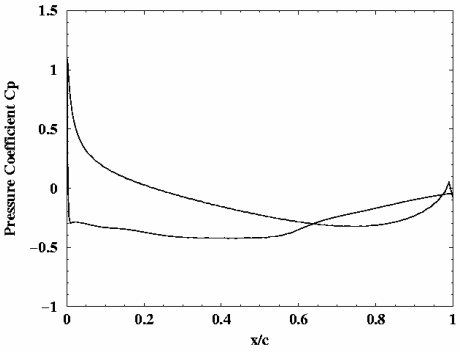

Fig. 7 Time averaged pressure coefficient under cavitating condition (σ =0.4)

Cavity Characteristics. The simulation results indicate the cavity generated on this foil under cavitation number of 0.8 and 0.4 is that of stable sheet cavity type. Although the lift coefficient fluctuates considerably and the flow is obviously unsteady, the periodical shedding of cloud cavity observed on NACA0015 foil is absent in this case. Typical instantaneous

pressure contour plots of a cavitating hydrofoil 2003 at cavitation numbers 0.8 and 0.4, respectively, are presented in figures 8 and 9. A region of nearly constant pressure indicating sheet cavity is clearly observable from these figures. Therefore, the geometry of sheet cavity is easily obtained from these figures. Similar pressure contour plots at different instants shows that the sheet cavity is fairly stable. Some characteristic lengths of the cavity are measured from pressure contour plots and presented at table 2. The cavity lengths for both cavitation numbers (0.8 and 0.4) are in good agreement with their corresponding time averaged pressure coefficients as shown in figures 6 and 7.

Table 2 Various characteristic length of the cavity

	Cavitation number 0.8	Cavitation number 0.4
$\bar{l}_d$	3.7%	5.6%
$\bar{t}_{\max}$	7.4%	22.2%
$\bar{l}_{\max}$	22%	62%
$\bar{l}_{t\max}$	50%	71%

Where $\bar{l}_d$, $\bar{t}_{\max}$, $\bar{l}_{t\max}$ and $\bar{l}_{\max}$ are defined as follows

$$\bar{l}_d = \frac{l_d}{c}$$
$$\bar{t}_{\max} = \frac{t_{\max}}{c}$$
$$\bar{l}_{\max} = \frac{l_{\max}}{c} \quad , \qquad (28)$$
$$\bar{l}_{t\max} = \frac{l_{t\max}}{l_{\max}}$$

and l_d, $t_{\max}$, $l_{\max}$ and $l_{t\max}$ are defined in figure 10.

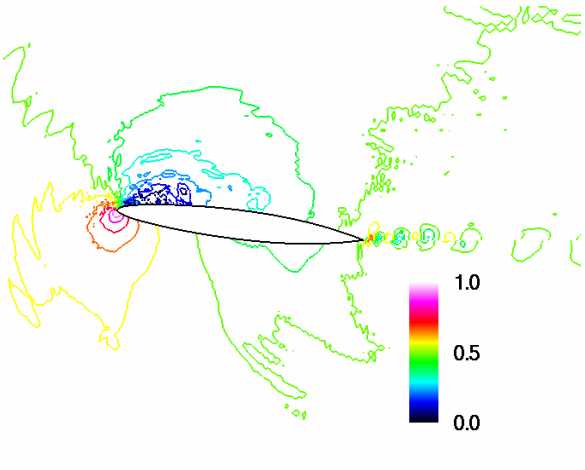

Fig. 8 Instantaneous pressure contour plot at cavitation number 0.8

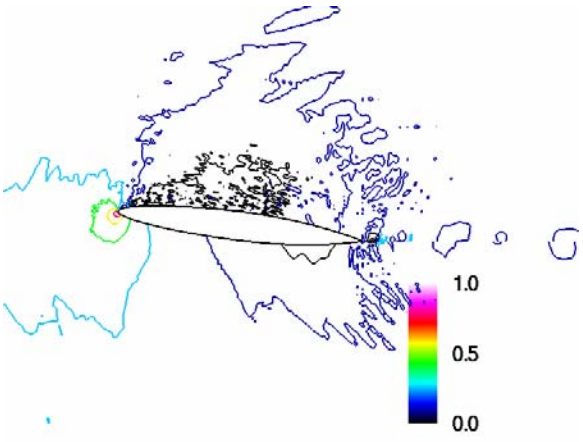

Fig. 9 Instantaneous pressure contour plot at cavitation number 0.4

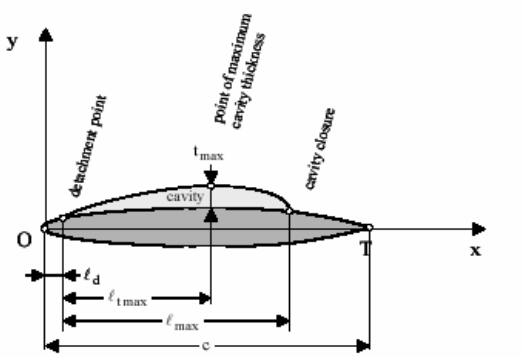

Fig. 10 Definition of various cavity characteristic lengths

Concluding Remarks

The details of virtual single-phase natural cavitating flow model are first presented and its application to Cav2003 hydrofoil shows that this model is able to capture the major dynamics of natural cavitating flows. The data about the cavity geometry is approximate because they are measured based on pressure distribution rather than based on photograph. Because of rather sharp nose, there is a rather sharp negative pressure peak near the nose on the suction side. The resulting adverse pressure gradient causes the boundary layer for non-cavitating condition to separate at about 70% chord. On the other hand, the sharp nose appears to make the cavitation inception to occur at a fixed point near the nose resulting in more stable sheet cavity. The cavity occurring at cavitation number of 0.8 and 0.4 appears to be the stable sheet cavity type and the periodical sheet/cloud cavity observed with NACA0015 foil is not observed here.

There is a region near the trailing edge of the foil where pressure on suction side is greater than that of the pressure side. This condition reduces the lift and the efficiency of the foil as a lifting body. Further study is needed to understand this phenomenon better.

Acknowledgements

This project is supported by the National Science Foundation (Dr. Michael Plesniak) and the Office of Naval Research (Dr. Kam Ng). The Minnesota Supercomputing Institute (MSI),

University of Minnesota, generously provides the computational resources.

References

[1] Batchelor, G.K. *An Introduction to Fluid Dynamics*, Cambridge University Press, 1967

[2] Brennen, C. *A Numerical Solution of Axisymmetric cavity flows*, Journal of Fluid Mechanics 37, 671-688, 1969

[3] Callenaere, M., Franc, J., Michel, J. and Riondet M. *The Cavitation Instability Induced by the Development of a Re-entrant Jet*, Journal of Fluid Mechanics, 444, 223-256, 2001

[4] Chen, Y. and Heister, S.D. *A Numerical Treatment for Attached Cavitation*, Journal of Fluid Engineering, 116, 613-618, 1994

[5] Chen, Y., Heister, S.D. *Modeling Hydrodynamic No-equilibrium in Cavitating Flows*, Journal of Fluid Engineering 118, 172, 1996

[6] Coutier-Delgosha, Q., Fortes-Patella, R. and Reboud, J.L. *Evaluation of the Turbulence Model Influence on the Numerical Simulation of Unsteady Cavitation*, Journal of Fluids Engineering, 125, 38-45, 2003

[7] Deshpande, M., Feng, J., Merkle, C.L. *Numerical Modeling of the Thermodynamic Effects of Cavitation*, Journal of Fluid Engineeing 119, 153, 1997

[8] Delannoy, Y., Kueny, J.L. *Cavity Flow Predictions Based on the Euler Equations*, ASME Cavitation and Multi-phase Flow Forum 109, 153, 1990

[9] Franc, J-P. and Schnerr, G.H. *Forum on Physical Models and CFD Tools for Computation of Cavitating Flows*, 5th International Symposium on Cavitation Website, Osaka, Japan, 2003

[10] Furness, R.A. and Hutton, S.P. *Experimental and Theoretical Studies of Two-dimensional Fixed-type Cavities*, Journal of Fluids Engineering, 97, 515-522, 1975

[11] Germano, M., Piomelli, U., Moin, P. and Cabot, W. *A Dynamic Subgrid-Scale Eddy Viscosity Model*, Physics of Fluids, 1760-1765, 1991

[12] Gopalan, S. and Katz, J. *Flow Structure and Modeling Issues in the Closure Region of Attached Cavitation*, Physics of Fluids, 12(4), 895-911, 2000

[13] Hoeijmakers, H.W.M., Janssens, M.E. and Kwan, W. *Numerical Simulation of Sheet Cavitation*, Proceedings of 3rd Internatinoal Symposium on Cavitation, Grenoble, France, 1998

[14] Inger, M.S. and Hailey, C.E. *A Numerical Approach for Modeling Cavitating Flows*, Computational Modeling of Free and Moving Boundary Problems, Proceedings of the First International Conference, Southampton, UK, 1991

[15] Lemonnier, H. and Rowe, A. *Another Approach in Modeling Cavitation, Journal of Fluid Mechanics*, 195, 557-580, 1988

[16] Lee, C.S., Kim Y.G., Lee, J.T. *A Potential-based Panel Method for the Analysis of a Two-dimensional Super- or Partially-cavitating Hydrofoils*, Journal of Ship Research 36, 168-181, 1992

[17] Kinnas, S.A. and Fine, N.E. *A Numerical Nonlinear Analysis of the Flow around Two- and Three-Dimensional Partially Cavitating Foils*, Journal of Fluid Mechanics, 254, 151-181, 1993

[18] Kubota, A. Kato, H., Yamaguchi, H. *A New Modeling of Cavitating Flows: A Numerical Study of Unsteady Cavitation on a Hydrofoil Section*, Journal of Fluid Mechanics 240, 59, 1992

[19] Kunz. R.F., Boger, D., Chyczewski, T., Stinebring D. and Gibling H. *Multi-phase CFD Analysis of Natural and Ventilated Cavitation about Submerged Bodies*, 3rd ASME/JSME Joint Fluids Engineering Conference, San Francisco, 1999

[20] Kunz. R.F., Boger, D., Stinebring D., Chyczewski, T., Lindau J.W. and Gibling H. *A Preconditioned Navier-Stokes Method for Two-phase Flows with Application to Cavitation Prediction*, Computers & Fluids, 29, 849-975, 2000

[21] Merkle, C.L. Feng, J. and Buelow P.E.O. *Computational Modeling of the Dynamics of Sheet Cavitation*, Proceedings of 3rd International Symposium on Cavitation, Grenoble, France, 1998

[22] Peck, B., Sigurdson, L. *the Creation of Vorticity at Fluid Interfaces*, APS Conference, 1996

[23] Pellone, C., Rowe, A. *Supercavitation Hydrofoils in Nonlinear Theory*, 3rd International Conference on Numerical Ship Hydrodynamics, Paris, France, 1981

[24] Piomelli, U. *Large-Eddy Simulation: Achievements and Challenges*, Progress in Aerospace Sciences 35(4), 335-362, 1999

[25] Shah, Y.T., Pandit, A.B. and Moholkar, V.S. *Cavitation Reaction Engineering*, Kluwer Academic / Plenum Publishers, 1999

[26] Senocak, I., Shyy, W. *A Pressure-Based Method for Turbulent Cavitating Flow Computations*, Journal of Computational Physics 176, 363-383, 2002

[27] Song, C.C.S. *Compressible Boundary Layer Theory and its Significance in Computational Hydrodynamics,* Journal of Hydrodynamics, series B, Vol. 8, No. 2, 1996

[28] Song, C.C.S. and He, J. *Numerical Simulation of Cavitating Flows with a Single-Phase Approach*, Proceedings of 3rd International Symposium on Cavitation, Grenoble, France, 1998

[29] Song, C.C.S. and Yuan, M. *A Weakly Compressible Flow Model and Rapid Convergence Methods*, Journal of Fluids Engineering, 110, 441-445, 1988

[30] Uhlman, J.S. The Surface Singularity Method Applied to Partially Cavitating Hydrofoils, Journal of Ship Research, 32(2), 107-124, 1987